

Two Methods for Random Shaker Testing with Low Kurtosis

Alexander Steinwolf, AST Consulting, Auckland, New Zealand

Non-Gaussian random vibration testing with kurtosis control has been known as a way of increasing the excitation crest factor, more realistically simulating ground vehicle vibrations and other situations when the time history includes extreme peaks higher than those of a Gaussian random signal. The opposite action may also be useful in other applications where a lower crest factor is desired. This article reviews two methods of kurtosis control, *polynomial transformation* and *phase selection*. We will show that non-Gaussian phase selection during inverse fast-Fourier transform (IFFT) signal generation can reduce kurtosis to 1.7 and bring the crest factor from 4.5 to 2. The phase selection method does this without any loss of the controller's dynamic range that inevitably occurs with polynomial transformation of time histories.

Shaker controllers for random vibration testing can be based on the well-established FFT/IFFT method.^{1,2} In this application, the test is specified in the frequency domain by a power spectral density (PSD), and actual time histories are reconstructed from the prescribed PSD by the inverse Fourier transform. It means that the shaker is driven by a multifrequency signal with a large number of harmonics, N :

$$x(t) = \sum_{n=1}^N A_n \cos(2\pi n\Delta f t + \phi_n) \quad (1)$$

The amplitudes, A_n , of the harmonics are determined

$$A_n = \sqrt{2\Delta f S(n\Delta f)} \quad (2)$$

according to the given PSD shape, $S(f)$, that is discretized with the frequency increment, Δf . The phase angles, ϕ_n , are defined as samples of a random variable uniformly distributed in the range from 0 to 2π radians. If a different set of phase values is used in each sequential data block generated according to Eq. (1), then the excitation obtained is a pseudo-random signal. It has a discrete power spectrum but, if necessary, a technique of windowing and overlapping time history blocks can be implemented¹⁻³ to make the resulting signal closer to true-random with a continuous spectrum.

The discrete Fourier transform model works well for digital random controllers. It allows easy correction of the input PSD shape using the acceleration feedback signal collected from the unit under test. A closed-loop iteration procedure is arranged to control the PSD of the shaker test vibration. The height of a certain spectral line, $S_i^{acc}(n\Delta f)$, located at the frequency $f=n\Delta f$ in the acceleration feedback PSD on i -th iteration, may become more (or less) than what it should be according to the test specification, $S_{spec}(n\Delta f)$, at this frequency. To compensate for the difference between $S_i^{acc}(n\Delta f)$ and $S_{spec}(n\Delta f)$, the height of the spectral line, $S_{i+1}^{dr}(n\Delta f)$, in the drive signal PSD on the next ($i+1$) iteration should be decreased (or increased) compared to the previous iteration value $S_i^{dr}(n\Delta f)$. Mathematically, this can be expressed as:

$$S_{i+1}^{dr}(n\Delta f) = S_i^{dr}(n\Delta f) \frac{S_{spec}(n\Delta f)}{S_i^{acc}(n\Delta f)}, \quad n = 1, 2, 3, \dots, N \quad (3)$$

Equation 3 is repeated for each of N spectral lines within the drive signal PSD for the next iteration. Then all discrete spectrum values, $S_{i+1}^{dr}(n\Delta f)$, obtained are substituted into Eq. 2, and a new drive signal time history is generated according to Eq. 1. Such iterations can be continued until the acceleration feedback spectrum, $S_i^{acc}(n\Delta f)$, is within desired tolerance of the specified target profile, $S_{spec}(n\Delta f)$.

This classic technique for simulating random excitations on

shakers can be updated to involve non-Gaussian characteristics such as kurtosis, which can be controlled in the same closed-loop iterative manner as the PSD.³⁻⁶ If the kurtosis value, K_i^{dr} , of the shaker drive signal is increased or decreased, the kurtosis of the acceleration feedback, K_i^{acc} , will follow it. So the kurtosis can be adjusted similarly to the height of a PSD line:

$$K_{i+1}^{dr} = K_i^{dr} \frac{K_{spec}}{K_i^{acc}} \quad (4)$$

with only one such correction for the entire random signal, not N corrections as for the PSD.

Leading controller manufacturers such as Vibration Research, Unholtz-Dickie, MB Dynamics, and IMV (Japan) have recognized the need for a non-Gaussian random testing approach and have started using it.⁷⁻¹⁰ Currently, their commercial implementations are restricted to increasing kurtosis only. The motivation for this objective was established in References 3,4,5,7,10. However, is it possible to go the other way and decrease kurtosis to generate a shaker excitation still with the given PSD but having a time history smoother than Gaussian? Will a smaller kurtosis value really lead to shaker vibration with less distinctive peaks; that is, with a lower crest factor? If yes, to what extent will the crest factor be lowered? These are the questions addressed here.

Kurtosis and Crest Factor

Implementation of non-Gaussian random simulation in vibration testing means controlling a much wider diversity of probability distributions of the generated excitations. Various deviations from the Gaussian model can be considered but this study focuses on controlling the probability of the occurrence of high-amplitude time history peaks. In other words, we look at how frequent and distinctive high peaks are in a time history block of a limited length. That is characterized by the kurtosis parameter:

$$K = \frac{M_4}{\sigma^4} = \frac{1}{\sigma^4} \int_{-\infty}^{\infty} x^4 P(x) dx \quad (5)$$

Kurtosis is associated with the fourth central moment M_4 of the signal's probability density function (PDF) denoted $P(x)$ in Eq. 5. The root-mean-square (RMS) value, σ , of the signal is also involved.

If the Gaussian PDF, $P_G(x) = \exp(-x^2 / 2\sigma^2) / (\sigma\sqrt{2\pi})$, is substituted into Eq. 5, the integral results in $3\sigma^4$, thereby making the kurtosis value equal to 3, regardless of the RMS value, σ . So if a random signal is Gaussian, then $K=3$ is the exact theoretical value for its kurtosis. If the signal is non-Gaussian with more frequent high-amplitude peaks, then $P_{nG}(x) > P_G(x)$ for large arguments x . With such an increase, the integration in Eq. 5 results not in $3\sigma^4$, but more, making the kurtosis $K > 3$. In the opposite case of $P_{nG}(x) < P_G(x)$, the corresponding kurtosis value is $K < 3$.

Kurtosis is a useful alternative to the common crest factor characterization of a signal. The crest factor is the ratio of the absolute maximum of a signal to its RMS value. That is:

$$CF = \frac{|x(t)|_{\max}}{\sigma} \quad (6)$$

The kurtosis parameter (Eq. 5) is more robust because, being an integral-based characteristic, it summarizes the effect of various extreme peaks. The crest factor (Eq. 6) is not as comprehensive; it takes into account only a single peak, the largest in the captured time history. Furthermore, in contrast to kurtosis, no strict theoretical value can be defined for the crest factor of a Gaussian signal because the magnitude of the largest peak depends on the length

of a time history sample.

Therefore, it is harder to quantify non-Gaussian deviations in terms of crest factor than in terms of kurtosis. In practice, for record lengths typical in shaker testing, $CF=4-4.5$ can be considered as corresponding to the Gaussian kurtosis value $K_G=3$. It is most important to note that for non-Gaussian random signals, the kurtosis and the crest factor follow the same pattern departing from the above values either up or down but both in the same direction.

Techniques for closed-loop random testing with kurtosis increase were developed first⁴⁻⁸ to raise the crest factor to realistically simulate ground vehicle vibrations and other situations when the time history includes excessive peaks higher than those appearing in Gaussian random signals. However, an opposite action of crest factor decrease may also be useful for other test specifications, including replacing sigma clipping.¹¹

Polynomial Transformation Can Decrease Kurtosis

The oldest method for generating a non-Gaussian signal is to generate a Gaussian time history using Eq. 1 as discussed earlier, and then to modify it using a functional transformation, $y = f(x)$, that converts digitized instantaneous values of the initial signal one by one into a new signal. The transformation can be conveniently prescribed in polynomial form with a third-order polynomial sufficient for kurtosis manipulations.

To increase kurtosis,^{5,12} let $x(t)$ be the standardized Gaussian signal (with zero mean and RMS equal to 1) and calculate the transform as:

$$y(t) = \alpha_1 x(t) + \alpha_3 x^3(t) \quad (7)$$

Then the cubic term governed by an appropriate choice of the coefficient α_3 will stretch those $x(t)$ values that are larger than 1. This action changes the distribution of instantaneous values, making higher peaks more prevalent. As a result, the transformed signal, $y(t)$, acquires higher kurtosis and crest factor.

To decrease kurtosis and crest factor, we need an opposite effect on the transformed signal so that it has peaks not as high as the original Gaussian signal. Actually, the same Equation 7 can be used^{12,13} to model the required change in peak behavior, but now $y(t)$ must be the standardized Gaussian signal, and $x(t)$ must become the required signal with lower kurtosis and crest factor.

For $K < 3$, an analytical solution was obtained¹³ for the coefficients α_1 and α_3 in terms of the desired kurtosis value, K_d :

$$\alpha_1 = h(1 - 3\beta), \quad \alpha_3 = h^3\beta \quad (8)$$

where:

$$h = \sqrt{1 + 42\beta^2}, \quad \beta = (3 - K_d)(35 - 9K_d) / 192$$

However, even with coefficients α_1 and α_3 determined, we do not really have the transform, since the controller needs a non-Gaussian instantaneous value, $x(t)$, to be calculated from the given Gaussian value, $y(t)$, not vice versa as in Eq. 7.

By solving Eq. 7 as an equation in $x(t)$, the required transformation function has been found in closed form. This is important for the controller's loop time. Actually, our functional transform for kurtosis decrease is not a polynomial transform, as was the case for kurtosis increase^{5,12} when using Eq. 7 directly. Nonetheless, the method continues to be called polynomial because it is still based on the polynomial relationship between the instantaneous values of the input and output signals involved.

Gaussian-to-non-Gaussian signal transformation was initially recommended¹² for preparing non-Gaussian time histories offline before running a test and then reproducing them on the shaker using the Time Waveform Replication mode. Later this approach was extended and modified^{5,6} into a method that could be used in the closed-loop frequency domain control mode. In this case, the polynomial transformation becomes just a post-IFFT signal processing addition, still within regular closed-loop FFT/PSD vibration testing procedures.

The polynomial transformation method (for both the kurtosis decrease discussed here and for the increase developed earlier) has an inherent tendency of introducing PSD distortions. This is of less concern if the PSD specification profile is such that a wide

dynamic range is not required from the controller, or if the test specification is mildly non-Gaussian and the harmonic distortions are not intolerably large. In these limited situations, the polynomial transformation method can be satisfactory.

However, generally speaking, PSD distortion is a major difficulty when using the polynomial transform. The problem can be avoided if two conditions are met. *Firstly*, changes to control the kurtosis should be done when generating the time history, not after the generation. *Secondly*, these changes should be administered by the use of parameters that do not affect the PSD. Since the power spectrum does not depend on harmonics phases, they can be manipulated to accomplish non-Gaussian simulation as discussed subsequently.

Kurtosis as a Phase-Controlled Parameter

The essence of the phase-selection method is that the variables are separated; amplitudes are still determined from the PSD according to Eq. 2. But the phases, ϕ_n , are not all randomly chosen. Instead, some of them are now used to adjust kurtosis. Thus, both characteristics, the PSD and the kurtosis, are controlled independent of each other. To achieve this, a general equation is needed for the kurtosis to be determined via the parameters involved in Eq. 1 for time history generation.

The fourth PDF moment, M_4 , that defines the kurtosis can be calculated not only in terms of the PDF as in Eq. 5, but also directly from the time history, $x(t)$:

$$M_4 = \frac{1}{T} \int_0^T \{x(t)\}^4 dt \quad (9)$$

A similar equation holds for a PDF moment of any order simply by changing the power superscript in the integrand. Particularly for the second moment, it will be $\{x(t)\}^2$ instead of $\{x(t)\}^4$. The second moment, M_2 , is actually RMS squared; i.e. $(M_2)^2$ can be used in Eq. 5 instead of σ^4 .

For a stationary ergodic random signal, the moment M_4 or that of any other order is found by Eq. 9 with the time history length, T , theoretically approaching infinity. However, for a pseudo-random signal generated according to Eq. 1, we use a finite data block whose length is $T=1/\Delta f$. Therefore, the fourth and other moments calculated using Eq. 9 are averaged over period T , not infinity.

Now Eq. 1 can be substituted into Eq. 9 or a similar equation for M_2 . If the integrals obtained are taken analytically, both moments M_2 and M_4 are expressed in terms of amplitudes A_n and phase angles ϕ_n . For the second moment:

$$M_2 = \frac{1}{T} \int_0^T \{x(t)\}^2 dt = \frac{1}{T} \int_0^T \left\{ \sum_{n=1}^N A_n^2 \cos^2\left(n\frac{2\pi}{T}t + \phi_n\right) + \sum_{n_1=1}^{N-1} \sum_{n_2=n_1+1}^N 2A_{n_1}A_{n_2} \cos\left(n_1\frac{2\pi}{T}t + \phi_{n_1}\right) \cos\left(n_2\frac{2\pi}{T}t + \phi_{n_2}\right) \right\} dt \quad (10)$$

integration poses no problem, because an integral of a product of two cosine functions from different harmonics with different subscripts (n_1 and n_2) is zero and an integral of $\cos^2\left(n\frac{2\pi}{T}t + \phi_n\right)$ over period T is equal to 0.5. Equation 10 results in the second moment, or the mean-square-value, σ^2 , being a function only of the *amplitudes* of the harmonics:

$$M_2 = \sigma^2 = \frac{1}{2} \sum_{n=1}^N A_n^2 \quad (11)$$

with the *phases*, ϕ_n , *uninvolved*.

It is much harder to derive an equation for the fourth moment, because the fourth power in the integrand in Eq. 9 produces cosine function products with more diverse combinations of harmonic indices n_1, n_2, \dots than in Eq. 10 which involves the second power. When all these combinations for M_4 are looked at, it appears that, after being integrated, many of them vanish similarly to the second term of the integrand function in Eq. 10. Some of the combinations result in sum functions involving only A_n^2 for all harmonics but no dependence on phases as in Eq. 11.

Distinct from the second moment, however, there will be non-zero components in M_4 that are functions of both amplitudes A_n

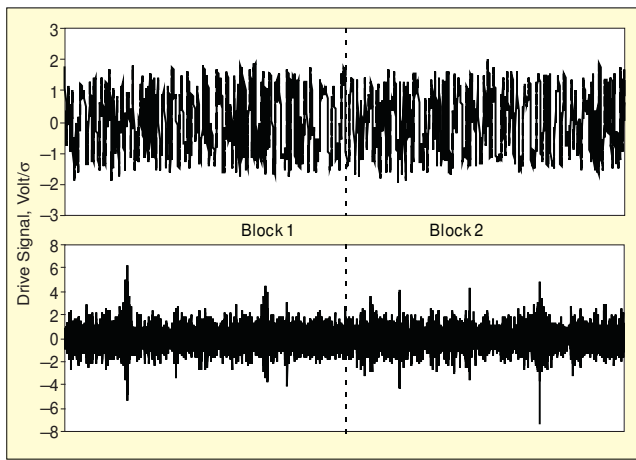


Figure 1. Each new data block is different in non-Gaussian signals

and phases φ_n . The structure of the fourth moment equation is:

$$M_4 = 3(M_2)^2 - \frac{3}{8} \sum_{n=1}^N A_n^4 + \frac{3}{2} \sum_{n_1=n_2+2n_3} A_{n_1} A_{n_2} A_{n_3}^2 \cos(\varphi_{n_1} - \varphi_{n_2} - 2\varphi_{n_3}) + \dots \quad (12)$$

Equation 12 is not the complete formula for M_4 . More terms need to be included that are also functions of amplitudes and phases as the third term in Eq. 12. The behavior of all these phase-dependent terms is similar, and we will discuss this using the last term in Eq. 12 as an example.

First, note that when calculating kurtosis by dividing Eq. 12 by $(M_2)^2$ according to the kurtosis definition, a value of 3 emerges from the first term in Eq. 12. This is true for any pseudo-random signal regardless of its amplitudes and phases. Thus, we are looking at something originating from the Gaussian kurtosis value, $K_G=3$, but different from it because of the contribution of the second and third terms in Eq. 12 and other phase-dependent terms not shown in Eq. 12.

The second term in Eq. 12 comes with a negative sign that reduces the kurtosis from 3, but this decrease is very small. For example, with 500 spectral lines in the PSD ($N=500$ in Eq. 1), the kurtosis is decreased by this second term from 3 to about 2.99. For more spectral lines, the change is even smaller. The exact value of a combination of the first two terms in Eq. 12 depends on the harmonic amplitudes A_n ; i.e. on the PSD shape. However, regardless of the PSD and the harmonic phases used to generate the pseudo-random signal, any changes in kurtosis are so small that they are within the precision of a kurtosis calculation from experimental data.

With only the first two terms in Eq. 12 taken into account, the kurtosis essentially remains the Gaussian value. It is the third and other similar terms omitted in Eq. 12 that make the kurtosis flexible. This is due to the fact that all these terms involve not only the harmonic amplitudes, A_n , but the phases, φ_n , as well. In the third term of Eq. 12, the argument of the cosine function is itself a function of phases φ_{n_1} , φ_{n_2} and φ_{n_3} of the same harmonic components that are present in the product of amplitudes $A_{n_1} A_{n_2} A_{n_3}^2$. All subsequent terms in the fourth moment equation that are not shown in Eq. 12 have similar structures.

Summation in the third and subsequent terms of Eq. 12 is performed only for those combinations of subscripts n_1, n_2, n_3 that satisfy conditions written under the summation symbol. Thus, the relationship between the harmonic subscripts n_1, n_2, n_3 such as:

$$n_1 = n_2 + 2n_3 \quad (13)$$

must be observed for this trio to form a member of the third sum in Eq. 12. For hundreds or even thousands of spectral lines in modern controllers, there will be plenty of subscript groups n_1, n_2, n_3 satisfying the condition set by Eq. 13.

If the phase angles, φ_n , of the harmonics are chosen in a random manner, as in the classical random control technique discussed previously, the cosine function in Eq. 12 also produces random values distributed uniformly in the interval from -1 to 1 . These random values, corresponding to different subscript groups, com-

pensate each other, bringing the result of summation close to zero as the number of groups is large.

The non-Gaussian phase selection method alters the aforementioned randomness of cosine function outputs by prescribing some of the phases in a certain deterministic way such that the corresponding term in Eq. 12 becomes positive or negative, instead of being close to zero. The outcome of such an action is that the kurtosis is increased or decreased from the Gaussian value, $K_G=3$. As it is only some of the phases that become deterministic, with the rest of them remaining random, each new data block generated according to Eq. 1 comes with a different set of harmonic phases.

The data blocks in the non-Gaussian signal are all different, as is the case for the classic Gaussian pseudo-random generation technique. The non-Gaussian time history never repeats itself, as seen in Figure 1, which depicts two signals: one (at the top) with $K=1.7$ and another (bottom) with $K=5$, with each containing two blocks of 4096 data points. The labels on the vertical axis correspond to $1\sigma, 2\sigma, 3\sigma, 4\sigma, \dots$ which is instrumental for observing the crest factor value. For the first signal, the crest factor was $CF=2.0$; for the second $CF=7.4$.

Effect of Kurtosis on Controller's Dynamic Range

Increasing or decreasing kurtosis using polynomial transformation introduces harmonic distortions to the drive signal. If, after a drive signal is IFFT-generated, any alterations – either polynomial transform or otherwise – are made to the time history, the drive signal spectrum will no longer correspond exactly to the target PSD. These changes in the PSD are spread over the entire frequency interval, including both the test specification bandwidth and out-of-band frequencies.

Some harmonic distortions caused by polynomial transformation can be compensated for in the closed-loop iteration process by decreasing the corresponding discrete PSD values $S_{i+1}^{dr}(n\Delta f)$ for the next iteration according to Eq. 3. But this does not work for the out-of-band frequencies or in the vicinity of sharp resonances. For the out-of-band frequencies, all spectral line amplitudes, A_n , are set to zero instead of being calculated by Eq. (2). At these frequencies, therefore, nothing contributes to generation of the time history and the discrete PSD values, $S_{i+1}^{dr}(n\Delta f)$, cannot be decreased further. If any PSD content is present at the out-of-band frequencies, it is caused by harmonic distortions only and will stay there as an uncontrollable “noise floor” in the PSD.

The harmonic distortions and the increased noise floor they produce affect not only the out-of-band frequencies. The shaker armature, test fixture, or the unit under test may have resonances where, according to Eq. 3, the controller will need very low $S_{i+1}^{dr}(n\Delta f)$ values in the drive signal PSD to match the required acceleration PSD specifications, $S_{spec}(n\Delta f)$, for this spectral line.

However, the controller output cannot be lower than the distortion-induced noise floor. Consequently, the noise floor level now determines the minimum PSD value that can be controlled. Clearly, if the PSD noise floor rises, then the controller's dynamic range (the difference between realizable maximum and minimum PSD values) will be reduced. This is the price paid for a simple non-Gaussian solution by using the polynomial transformation.

Shaker controller manufacturers regard dynamic range as one of the most important performance characteristics¹⁴⁻¹⁶ and report it to be in the region of 90 dB for modern Gaussian random controllers. A loss of available dynamic range should be expected if polynomial transformation is introduced for non-Gaussian random vibration testing. But what fraction of this 90 dB disappears when switching from Gaussian to polynomial non-Gaussian mode? And what happens to the dynamic range when using the phase selection non-Gaussian method?

To answer these questions, an experiment was carried out on a Derritron VP5/DLA1050 electrodynamic shaker controlled by a PC equipped with a National Instruments PCI-MIO-16E-4 DAQ board and LabView 7.0 software to accomplish digital-to-analog and analog-to-digital conversion of the signals. Kurtosis and crest factor were evaluated using data samples of 80 blocks of 4096 data points each. The power spectrum was analyzed with 2000 spectral lines and a frequency increment of $\Delta f=2$ Hz. The target

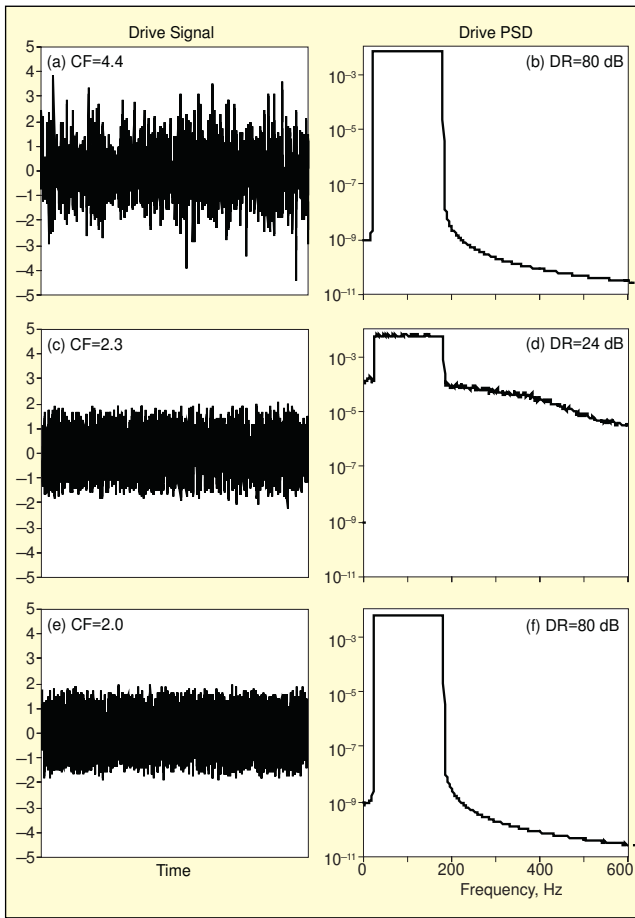


Figure 2. Drive signal characteristics: (a, b) Gaussian; (c, d) non-Gaussian by polynomial transform; (e, f) non-Gaussian by phase selection.

PSD profile was a uniform spectrum from 20 to 180 Hz and zero everywhere else.

Figure 2a shows a Gaussian drive signal that was used initially. This signal has a crest factor of $CF=4.4$. It can be seen in Figure 2b that the specified PSD profile was realized experimentally with the drive signal dynamic range, $DR=80$ dB. This drive input produced an acceleration output signal (Figure 3a) also with $CF=4.4$. The acceleration PSD obtained is shown in Figure 3b. Note the dynamic range of the output signal $DR=33$ dB. This value is less than in commercial controllers where special measures are taken to achieve higher dynamic range, but it is sufficient to see the tendencies discussed below.

Now look at how it all changes with the polynomial transform added to the standard Gaussian technique. The coefficients α_1 and α_3 in Eq. 7 were calculated according to Eq. 8 to decrease kurtosis of the drive signal to $K_f=1.7$. This resulted (see Figure 2c) in the crest factor reduced to $CF=2.3$ from the initial Gaussian value of $CF=4.4$ in Figure 2a. The non-Gaussian drive signal has produced an acceleration output signal (Figure 3c) with $CF=3.0$. It is a substantial decrease from $CF=4.4$ in Figure 3a, but there is a price to pay.

At the out-of-band frequencies, the acceleration PSD (Figure 3d) has a much higher level than that of the PSD of the Gaussian excitation in Figure 3b. About 70% of the control dynamic range has been lost, just 10 dB remaining instead of the initial 33 dB in Figure 3b. This is the result of the drive signal dynamic range in Figure 2d being only 24 dB rather than $DR=80$ dB for the Gaussian excitation in Figure 2b. That is typically what the non-Gaussian method of post-IFFT polynomial transformation can offer, and now it will be compared with the performance of the special phase selection method.

As previously discussed, the phase angles, ϕ_n , in the IFFT procedure can be manipulated so that the kurtosis value of the signal generated by Eq. 1 becomes lower. The amplitudes, A_n , remain responsible for the PSD as in the common Gaussian technique. That is what the phase selection method for non-Gaussian random

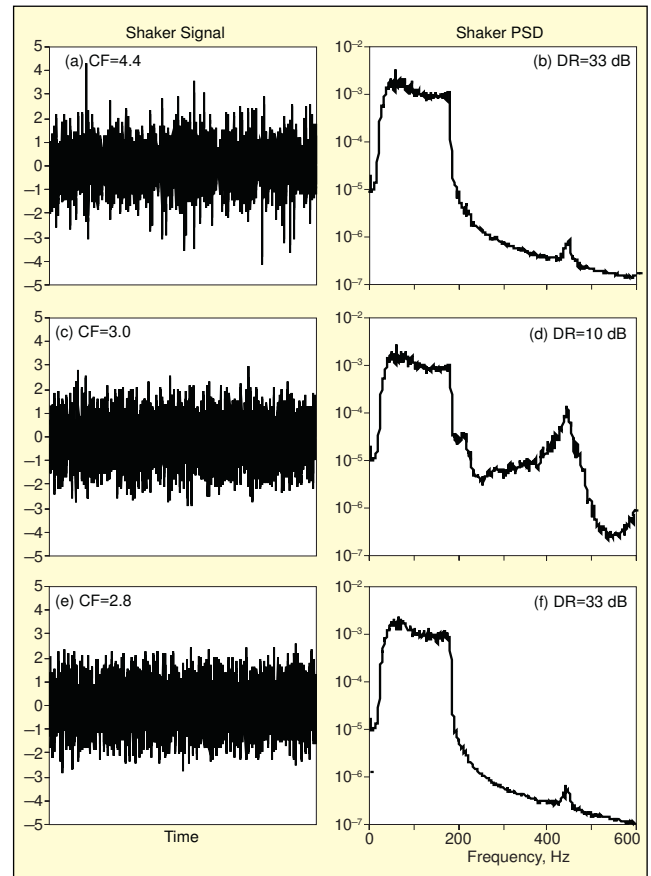


Figure 3. Shaker feedback characteristics: (a, b) Gaussian; (c, d) non-Gaussian by polynomial transform; (e, f) non-Gaussian by phase selection.

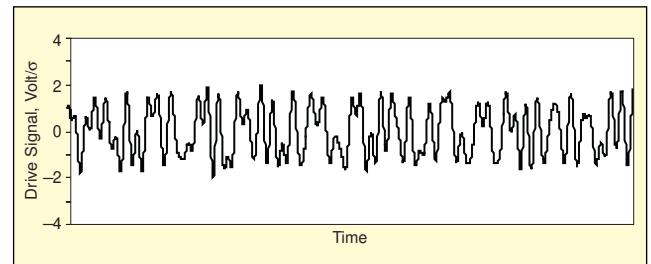


Figure 4. Fragment of non-Gaussian signal with kurtosis $K=1.7$ and crest factor $CF=2$.

shaker control is about. The results obtained by this method for the same experimental setup follow.

A non-Gaussian drive signal with kurtosis $K=1.7$ is shown in Figure 2e, and its magnified fragment is depicted in Figure 4. The signal was generated for the same target PSD profile as that used in the Gaussian and polynomial transformation experiments (Figures 2a, b, c and d and 3a, b, c and d). Now, with non-Gaussian phase selection control (Figure 2e), the crest factor is $CF=2.0$, which is much less than the value of $CF=4.4$ for the Gaussian drive signal in Figure 2a. Despite such a drastic time history modification, the PSD of the non-Gaussian drive signal (Figure 2f) has exactly the same low tail for out-of-band frequencies as that of the PSD of the Gaussian drive signal (Figure 2b).

The PSD noise floor for the non-Gaussian simulation using special phase selection (see Figure 2f) remains where it was for the traditional Gaussian simulation in Figure 2b. This means that the drive signal dynamic range is maintained (in this experiment at $DR=80$ dB). After the drive signal kurtosis decrease was achieved without compromising the out-of-band frequencies, we can expect that the dynamic range of the shaker acceleration signal will be as good as for the basic Gaussian simulation and this is confirmed by comparing Figures 3b and 3f.

As for the non-Gaussian acceleration time history (Figure 3e), its crest factor appears to be $CF=2.8$. The difference between this value

and $CF=3$ obtained with the post-IFFT polynomial transformation (Figure 3c) might look nonessential, but remember that the latter comes with the input and output dynamic ranges of 24 and 10 dB, while the phase selection method shows an impressive 80 and 33 dB, which are exactly the same as in the Gaussian mode!


Conclusions

Two methods of non-Gaussian, closed-loop random control for vibration testing have been suggested and realized experimentally, first for kurtosis increase, and now for kurtosis decrease. It is important that in both methods the PSD and kurtosis corrections can be done simultaneously in the same iteration procedure to save the controller's loop time.

The non-Gaussian method of post-IFFT polynomial transformation is easy to implement, but it significantly reduces the dynamic range of the controller system compared to traditional Gaussian random vibration testing. The dynamic range degradation is unavoidable with the polynomial transform, because *changes are made to the drive signal time history after it has been generated by the IFFT*, and this results in harmonic distortions.

Another, more advanced, non-Gaussian method by phase selection is different, since it decreases kurtosis and crest factor *not after but in the process of IFFT signal generation*. In so doing, the multifrequency character of the pseudo-random drive signal remains intact with absolutely no alterations from the combination of pure sinusoidal components. So there are no harmonic distortions passed to other frequencies, as is the case for polynomial transformation. The phase selection method allows us to generate shaker excitations with low kurtosis and crest factor while being able to preserve the same dynamic range and PSD precision as in conventional Gaussian random vibration controllers.

References

1. Sloane, E. A., and Heizman, C. L., Vibration Control System, *U.S. Patent 3,848,115*, Nov. 12, 1974.
2. Ueno, K., and Imoto, K., Vibration Control System, *U.S. Patent 5,012,428*, Apr. 30, 1991.
3. Steinwolf, A., "True-random Mode Simulation of Non-Gaussian Vibrations with High Kurtosis Value," Proceedings of the 46th IEST Annual Technical Meeting, p. 148-155, Providence, RI, 2000.
4. Steinwolf, A., "Shaker Simulation of Random Vibrations with High Kurtosis Value," *Journal of the Institute of Environmental Sciences*, Vol. XL, No 3, p. 33-43, 1997.
5. Steinwolf, A. "Random Vibration Testing Beyond PSD Limitations," *Sound & Vibration*, Vol. 40, No 9, p. 12-21, 2006.
6. Steinwolf, A., "Closed-Loop Shaker Simulation of Non-Gaussian Random Vibrations, Part 1, Discussion and Methods; Part 2, Numerical and Experimental Results," *Test Engineering and Management*, Jun/Jul, p. 10-13, Oct/Nov, p. 14-19, 2006.
7. Van Baren, J., and Van Baren, P., "The Third Dimension of Random Vibration Control," SAE Paper 2007-01-2270, Noise and Vibration Conference, St. Charles, IL, 2007.
8. "Non-Gaussian Random Control," Unholtz-Dickie News, www.udco.com/news.shtml/Gaussian.
9. Kawata, A., and Yamauchi, Y., "Non-Gaussian Random Vibration Testing Beyond the Conventional Testing – On the Progress of Mathematical Method," *Journal of Packaging Science & Technology*, Vol. 15, No 5, p. 237-243, 2006.
10. Trapp, M., and Peterson, E. L., "A Systematic Approach to Preparing Drive Files for Squeak and Rattle Evaluation of Subsystems or Components," SAE Paper 2007-01-2269, Noise and Vibration Conference, St. Charles, IL, 2007.
11. Steinwolf, A., "Forget Clipping: Go Random with Non-Gaussian Sigma Limiting and Double the Shaker Power," *Test Engineering and Management*, Vol. 69, No. 3, p. 10-13, 2007.
12. Smallwood, D. O., "Generating Non-Gaussian Vibration for Testing Purposes," *Sound & Vibration*, Vol. 39, No 10, p. 18-24, 2005.
13. Winterstein, S. R., Manuel, L., and Ness, O. B., "Nonlinear Dynamic Responses of Marine Structures Under Random Wave Loads," Proceedings of the 5th Int. Conference on Structural Safety and Reliability, San Francisco, p. 159-166, 1989.
14. Van Baren, P., and Lang, G. F., "Examining the Dynamic Range of Your Vibration Controller," *Sound & Vibration*, Vol. 41, No 8, p. 12-20, 2007.
15. "Control System Dynamic Range," Spectral Dynamics Technical Note, www.spectraldynamics.com/dynamic_range.htm.
16. "Control Dynamic Range," LDS/Dactron Technical Note, TN002, www.lds-group.com/docs/site_documents/TN002R2%20Control%20Dynamic%20Range.pdf. 

The author may be reached at: steinwolf@ihug.co.nz.